On-surface nickel porphyrin mimics the reactive center of an enzyme cofactor†

Giovanni Zamborlini, ‡*[a] Matteo Jugovac, [a] Albano Cossaro, [b] Alberto Verdini, [b] Luca Floreano, *[b] Daniel Lüftner, [c] Peter Puschnig, [c] Vitaliy Feyer *[a] and Claus M. Schneider [ad]

Metal-containing enzyme cofactors achieve their unusual reactivity by stabilizing uncommon metal oxidation states with structurally complex ligands. In particular, the specific cofactor promoting both methanogenesis and anaerobic methane oxidation is a porphyrinoid chelated to a nickel(I) atom *via* a multi-step biosynthetic path, where nickel reduction is achieved through extensive molecular hydrogenation. Here, we demonstrate an alternative route to porphyrin reduction by charge transfer from a selected copper substrate to commercially available 5,10,15,20-tetraphenyl-porphyrin nickel(II). X-ray absorption measurements at the Ni L_3-edge unequivocally show that NiTPP species adsorbed on Cu(100) are stabilized in the highly reactive Ni(I) oxidation state by electron transfer to the molecular orbitals. Our approach highlights how some fundamental properties of synthetically inaccessible biological cofactors may be reproduced by hybridization of simple metalloporphyrins with metal surfaces, with implications towards novel approaches to heterogenous catalysis.

The catalytic properties of metal-containing tetrapyrrolic compounds strongly depend on the oxidation state of the chelated metal ion.[1,2] In the case of surface-supported molecular systems, the degree of reactivity can be either reduced or enhanced due to charge transfer (CT). For example, gold substrates promote oxygen catalysis by Cu- and Fe-phthalocyanines (CuPc and FePc) *via* either direct or indirect (through backbonding to an intermediate molecular linker) charge transfer, respectively.[3] Similarly, gold promotes the reduction of MnCl-porphyrins so that they can be easily oxidized (MnOP) and subsequently employed for the on-surface alkene epoxidation.[4] In vacuum, one can even control the self-assembly geometry on inert metals in order to tune the degree of molecular reactivity, as demonstrated for oxygen reduction by FePc on silver.[5] Pioneering studies on two-dimensional (2D) organic frameworks have also shown the possibility of enhancing the reactivity of metal adatoms by entrapping them in a 2D network of small molecules, eventually reproducing the catalytic properties of natural enzymes,[6] as a result of the equilibrium between molecular and substrate charge transfer.[7]

In general, the metal center of tetrapyrroles adsorbed on metal surfaces is subject to charge transfer, whose extent depends on both the chelated metal species and the substrate reactivity.[8,9] Hence, one might increase the degree of porphyrin rehybridization by an appropriate choice of the substrate for preparing synthetic analogs of low valency metal-containing coenzymes. A prototypical example of such natural compounds is the F_{430} cofactor (Fig. 1a top), a porphyrinoid required by methyl-coenzyme M reductase (MCR) for catalyzing methane formation and the reverse anaerobic methane oxidation in archaeal prokaryotes.[10–12] The F_{430} coenzyme is a nickel(I)-containing tetrapyrrole, derived from the uroporphyrinogen III macrocycle through multiple biosynthetic processes.[13] In nature, the reduction of the F_{430} macrocycle, which is the key to its extremely high reactivity, is achieved through extended hydrogenation of the tetrapyrrole. While the chemical synthesis of F_{430} is a nearly intractable challenge, replication of its low-valence nickel center may be accomplished in strongly interacting organic/metal hybrid systems, where the overall physical and chemical properties of the interface are dramatically altered, due to chemical reactions and rehybridization triggered by charge transfer.[14,15]

Here, we propose nickel tetraphenyl porphyrin (NiTPP, Fig. 1a bottom) 2D arrays deposited on a Cu(100) surface as a model system to study the catalytic properties of a reduced Ni(I) center that mimics the oxidation state of the F_{430} cofactor. The reactivity of the NiTPP overlayer is further confirmed by the adsorption of nitric oxide, which reverts the oxidation state of the active site close to the pristine Ni(II) one.

In our previous work, we have shown that a strong interaction takes place between the NiTPP frontier orbitals and Cu(100),

[a] *Peter Grünberg Institute (PGI-6), Forschungszentrum Jülich GmbH, 52425 Jülich, Germany. E-mail: v.feyer@fz-juelich.de*
[b] *IOM-CNR Laboratorio TASC, S.S. 14 km 163.5 in AREA Science Park, Basovizza, 34149 Trieste, Italy. E-mail: floreano@iom.cnr.it*
[c] *Institut für Physik, Karl-Franzens-Universität Graz, NAWI Graz, 8010 Graz, Austria*
[d] *Fakultät für Physik and Center for Nanointegration Duisburg-Essen (CENIDE), Universität Duisburg-Essen, 47048 Duisburg, Germany*

† Electronic supplementary information (ESI) available. See DOI: 10.1039/c8cc06739b

‡ Present address: Technische Universität Dortmund, Experimentelle Physik VI, 44227 Dortmund, Germany. E-mail: giovanni.zamborlini@tu-dortmund.de

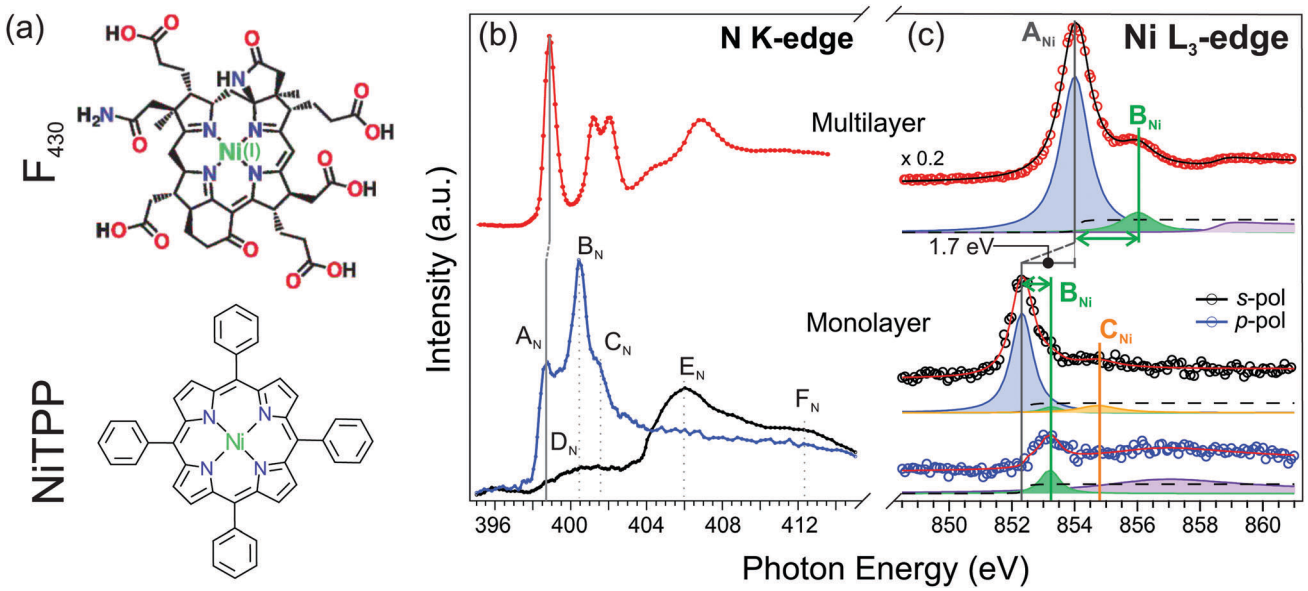

Fig. 1 The comparison between the chemical structures of coenzyme F_{430} and NiTPP can be appreciated in the top and bottom pictures of panel (a) respectively. The NEXAFS spectra at the N K-edge and the Ni L_3-edge are shown in panels (b) and (c), respectively; the spectra measured in both p and s polarizations on the NiTPP monolayer deposited on Cu(100) at room temperature are shown at the bottom; for comparison, the spectra measured in p polarization on a multilayer (~8 ML) grown at room temperature are also shown (top); the main resonances related to specific transitions to unoccupied states are labeled, and, for the Ni L_3-edge, the corresponding fit is superimposed on the graph.

which leads to the partial filling of the unoccupied molecular orbitals (MOs): from the LUMO to LUMO+3.[16] Here, we show that this strong CT to the molecular orbitals is enhanced at the chelated metal, resulting in an effective (II) → (I) reduction of its oxidation state. In this regard, NEXAFS spectroscopy at the nitrogen K-edge is a valuable tool to determine both the adsorption geometry and the electronic properties of the porphyrin macrocycle. In the NEXAFS K-edge spectra, the intensity of the core level electron transition to an unoccupied MO depends on the angle between the electric field of the linearly polarized incoming light and the spatial orientation of the unoccupied MOs. If molecules in the film display a preferential orientation, the NEXAFS resonances measured with the electric field oriented parallel (s-polarization) and perpendicular (p-polarization) to the surface will display different intensities (NEXAFS dichroism), according to the MO symmetry.

NEXAFS spectra at the N K-edge, recorded with s- and p-polarizations, are shown in Fig. 1b. In this case, it is possible to assign three absorption features related to the 1s → π* transitions (A_N–C_N) and other three associated with 1s → σ* ones (D_N–F_N).[17,18] In particular, the two low energy features A_N and B_N are mainly related to the transition of N 1s electrons to the degenerate LUMO/LUMO+1 (LUMO/+1) and LUMO+3 orbitals.[17,18] The resonance D_N, which is well pronounced in the s-pol NEXAFS spectrum, is attributed to the transition from the N 1s to LUMO+2 orbital, a σ-symmetry molecular state. The prominent shoulder C_N, instead, corresponds to the electron transition from the 1s shell to higher LUMOs. All π* and σ* resonances show a strong polarization dependence (large dichroism): while the former (A_N, B_N and C_N) are enhanced in p-pol and almost vanish in s-pol, the latter (D_N, E_N and F_N) have the opposite behaviour. Since the sharp π* resonances in the spectra originate from the four pyrrolic nitrogens of the macrocycle, we can conclude that the NiTPP macrocycle is closely planar and lies almost parallel to the copper surface. The N K-edge spectra at the monolayer coverage display a large quenching of the LUMO/+1 (A_N), as well as an overall shift to a lower energy of the whole spectrum with respect to the multilayer one. Both effects are associated with a partial filling of the corresponding MOs, due to the strong charge transfer from the substrate.[19–21] We notice that a similar intensity decrease of the first resonance has also been reported for CuTPP and H_2TPP monolayers deposited on Cu(111),[17] suggesting that a relatively large CT to both metalated and free-base porphyrins is common to copper surfaces for any crystallographic orientation.

The partial filling of several unoccupied MOs affects the electronic structure of the entire NiTPP macrocycle; in particular, the charge transferred from the substrate to the molecule may reduce the Ni ion. In fact, X-ray Photoemission Spectroscopy (XPS) measurements of the Ni 2p core level of the monolayer phase display a significant shift to lower binding energies (~2.8 eV) with respect to the multilayer one (Fig. S1 of the ESI†). The corresponding binding energy agrees well with the reported values for NiTPP on reactive surfaces such as Cu(111)[22] and fcc Co(100)/Cu(100),[23] and closely matches the binding energy of metallic nickel.[24] On metals, the XPS core level shift (CLS) of the adsorbates cannot directly provide a quantitative indication of the corresponding oxidation state, because it also contains a contribution from the sudden screening of the core-hole by substrate Fermi electrons. Such a screening CLS contribution is typically found in the range of few tenths of eV, while values exceeding 1 eV rather originate from static charge transfer between the metal and the adsorbate; however, complementary measurements are required for a more quantitative analysis of

the electronic configuration of chelated Ni and the corresponding rehybridization of the molecular orbital. For this reason, in order to get direct access to the oxidation state of the Ni atom, we acquired absorption spectra for both multi- and monolayer NiTPP coverages at the Ni L_3 edge (Fig. 1c, top and bottom, respectively). In fact, the shape of the NEXAFS spectrum (*i.e.* the relative position and intensity of the resonances) does not depend on the substrate charge screening and it is a very sensitive probe of the Ni electronic configuration,[25,26] down to the fine details of the corresponding molecular orbital.[18] The NEXAFS spectra of the thicker NiTPP film do not show any polarization dependence, indicating that molecules in the topmost layers are randomly oriented with respect to the surface. The detailed analysis of the spectral features of the porphyrin in the multilayer film shows an energy separation of ~2 eV between the main peak A_{Ni} and its satellite feature B_{Ni} (energy positions of 854.0 eV and 856.0 eV, respectively). These values and the spectral shape are a fingerprint of the Ni(II) coordination within the porphyrin macrocycle. The main peak is associated with a σ*-symmetry intra-atomic transition ($2p_{3/2} \rightarrow 3d_{x^2-y^2}$) and the satellite B_{Ni} is assigned to π*-symmetry transition to unoccupied MOs resulting from the hybridization of Ni 3d and ligand p states.[18]

Comparing the multilayer to the monolayer spectra, we notice a dramatic change in both the line-shapes and energy positions of the observed features. The main peak A_{Ni} is shifted to a lower photon energy by ~1.7 eV (852.3 eV). We observe an even larger shift by ~2.8 eV of the satellite B_{Ni} (853.2 eV, see Fig. 1c bottom) corresponding to an energy separation ($A_{Ni} - B_{Ni}$) of ~0.9 eV. The details of the best fitting parameters are shown in Table S1 of the ESI.† In contrast to the multilayer, the Ni L_3-edge NEXAFS for the NiTPP monolayer shows a strong polarization dependence: A_{Ni} is enhanced in the s-pol spectrum and vanishes for the other polarization. The satellite feature B_{Ni} displays a reversed NEXAFS dichroism, being maximum in p-polarization and minimum (yet not vanished) in s-polarization (see Fig. 1c, bottom). The overall NEXAFS dichroism is consistent with the expected σ*-symmetry of the peak A_{Ni} corresponding to a closely planar macrocycle oriented parallel to the surface. This geometric configuration is fully consistent with the quantitative analysis of the NEXAFS dichroism at the N K-edge, reflecting the orientation of the tetrapyrrolic macrocycle. The C K-edge spectra additionally reveal that the phenyls are tilted off the surface by ~70° (see Fig. S2 of the ESI†). In contrast, the B_{Ni} satellite has a dominant π*-symmetry character. The latter orbital displays a shift to lower binding energy even larger than that of A_{Ni}, and also a residual intensity in s-polarization. Both effects suggest a re-hybridization with the substrate of the corresponding mixed Ni 3d-ligand p molecular state due to charge transfer at the interface, in full agreement with the analysis of the corresponding π*-symmetry orbitals at the N K-edge.

In Fig. 2 we compare the projected density of states (PDOS) on the first unoccupied molecular orbitals (top) with the one on the Ni d-states (bottom). The energy positions of the gas-phase MOs are marked with colored bars in the upper part of the graph. Upon adsorption, the molecular orbitals spread over a wide energy range. In particular, the degenerate LUMO/+1 shifts below the Fermi level (E_F), becoming almost entirely

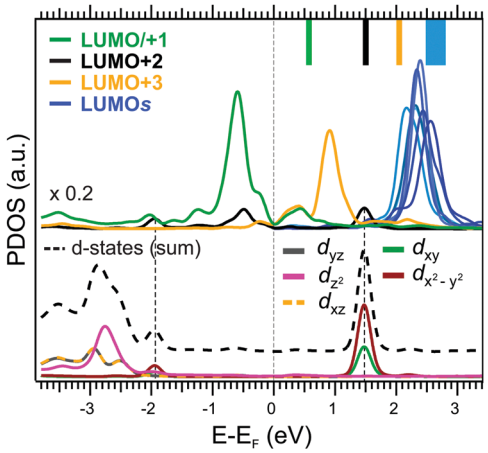

Fig. 2 (Top) PDOS onto molecular orbitals for the NiTPP/Cu(100) system, from degenerate LUMO/+1 to LUMO+10. The energy positions of the corresponding gas-phase molecular orbitals, aligned with respect to the vacuum level, are indicated with colored bars on the top axis. (Bottom) The DOS of NiTPP/Cu(100) projected onto the Ni d-states.

filled, while LUMO+2, which has a strong σ character, spreads over a few eV across E_F. We now focus on the state located 1.5 eV above the Fermi energy (marked with a dashed line). This component is mainly located on the Ni ion at the macrocycle centre. No other MOs are located at this energy, while the PDOS on the Ni d-states shows a prominent peak. The only two d-states that contribute to this peak are the σ*-symmetry orbitals d_{xy} and $d_{x^2-y^2}$. This indicates that the σ-symmetry LUMO+2 component above E_F is mostly localized on the Ni atom, in full agreement with the polarization dependence of the A_{Ni} peak at the Ni L_3-edge. Overall, the energy shift of the A_{Ni} resonance, together with the change in the Ni L_3-edge lineshape, is consistent with a change in the Ni oxidation state, namely reduction, of the molecules at the interface with Cu(100).[27] In the specific case of nickel, extensive NEXAFS mapping in many different compounds has shown that the L_3 X-ray absorption centroid is a good indicator of the Ni oxidation state: a weighted position of the A_{Ni} (~852.5 eV) and B_{Ni} features (~853.5 eV) is characteristic of the nickel(I) valence state.[28] This assignment is also in agreement with the observed shape of the Ni(I) L_3-edge spectrum,[26] which is dominated by a single peak (closely corresponding to the centroid) with a close shoulder (please note that spectra shown in ref. 26 are not symmetry resolved like the present one), while the broad features at higher energies (>2–3 eV) depend on the details of the specific molecular bonds.[25,29] Finally, the observed large shift of the B_{Ni} satellite indicates that the reduction involves the molecular orbital of the NiTPP macrocycle as a whole. These lines of evidence, all together, point to a direct comparison of the NiTPP reduced molecule with the characteristics of the active centre of the MCR enzyme responsible for methane formation and consumption. The reactivity of MCR is known to be attributed to the specific Ni(I) valence state of its F_{430} porphyrinoid cofactor (two of them in each MCR molecule, as prosthetic groups),[30,31] whereas the other two MCR forms mostly found in the purified enzyme, Ni(II) and Ni(III), are inactive. In fact, the search for conversion of the MCR-Ni(II) form into the MCR-Ni(I)

form is a challenging task due to the high sensitivity to O_2 of the reduced F_{430} active center.[32,33] In the past, alternative chemical routes have been followed to stabilize nickel in its Ni(I) oxidation state, such as chelation of thioethers, where Ni is coordinated to four sulfur atoms in a planar square geometry.[34] Remarkably, tetraplanar coordination of Ni adatoms to the nitrogen terminations of a 2D network of tetracyanoquinodimethane is also responsible for the observed predominant Ni $3d^9$ character.[7] Hence, a homoleptic tetraplanar square configuration is a common aspect of Ni(I) compounds, whose final reduction is achieved either through specific functionalization of the chelated species (F_{430} and Ni(I)tetrathioether species) or through substrate mediated charge transfer like for NiTPP on Cu(100). In the present case, the effective reactivity of the Ni(I)TPP overlayer was tested by exposing it to a toxic gas, namely nitric oxide (NO). The significant changes in the NEXAFS spectra measured at the Ni L_3-edge (Fig. S3 of the ESI†) reveal the co-adsorption of NO at the Ni(I) active site. In particular, we observed a combined shift to higher energy of both the main peak A_{Ni} and, to a larger extent, of its satellite B_{Ni}. The resulting shape of the NEXAFS spectrum closely resembles that of the multilayer Ni(II)TPP, apart from a residual shift of $\sim$1 eV, indicating an effective re-oxidation of the nickel ion. As a consequence, the possibility of stabilizing a supported layer of Ni(I)-TPP on copper offers an alternative approach to the dissociation and/or synthesis of highly reactive molecules in a system suitable for heterogeneous catalysis.

In conclusion, we have artificially obtained a 2D array of reduced nickel(I) tetrapyrrole compounds by adsorbing commercially-available Ni(II)-TPP molecules atop the Cu(100) surface. This interface has been characterized by means of NEXAFS and XPS spectroscopy, supported by DFT calculations. The shift and line shape change in the Ni L-edge absorption spectra prove a (II) $\rightarrow$ (I) reduction of the Ni ion at the porphyrin macrocycle center, which is promoted by large charge transfer from the copper surface to the molecular film. Furthermore, the quenching of the π^* and σ^* resonances in the N K-edge absorption spectra indicates: electron transfer to the unoccupied MOs up to LUMO+3. This so-obtained self-assembled low-valence nickel array may represent a model for more complex systems, such as the F_{430} cofactor of the MCR enzyme, and can open a pathway towards the study of bio-related processes involving methanogenesis catalysis and anaerobic methane oxidation within the surface science framework.

The authors thank Jeff Rawson for helpful discussions. D. L. and P. P. acknowledge support from the Austrian Science Fund (FWF) project P27649-N20. All computational results were achieved using the computing facilities of the University of Graz and the Vienna Scientific Cluster (VSC3).

Conflicts of interest

There are no conflicts to declare.

Notes and references

1 D. den Boer, M. Li, T. Habets, P. Iavicoli, A. E. Rowan, R. J. M. Nolte, S. Speller, D. B. Amabilino, S. De Feyter and J. A. A. W. Elemans, *Nat. Chem.*, 2013, **5**, 621–627.
2 B. A. Friesen, A. Bhattarai, U. Mazur and K. W. Hipps, *J. Am. Chem. Soc.*, 2012, **134**, 14897–14904.
3 I. Ponce, J. F. Silva, R. Oñate, M. C. Rezende, M. A. Paez, J. H. Zagal, J. Pavez, F. Mendizabal, S. Miranda-Rojas, A. Muñoz Castro and R. Arratia-Pérez, *J. Phys. Chem. C*, 2012, **116**, 15329–15341.
4 B. Hulsken, R. Van Hameren, J. W. Gerritsen, T. Khoury, P. Thordarson, M. J. Crossley, A. E. Rowan, R. J. M. Nolte, J. A. A. W. Elemans and S. Speller, *Nat. Nanotechnol.*, 2007, **2**, 285–289.
5 F. Sedona, M. Di Marino, D. Forrer, M. Casarin, A. Cossaro, L. Floreano, A. Verdini and M. Sambi, *Nat. Mater.*, 2012, **11**, 970–977.
6 R. Gutzler, S. Stepanow, D. Grumelli, M. Lingenfelder and K. Kern, *Acc. Chem. Res.*, 2015, **48**, 2132–2139.
7 N. Abdurakhmanova, T.-C. Tseng, A. Langner, C. S. Kley, V. Sessi, S. Stepanow and K. Kern, *Phys. Rev. Lett.*, 2013, **110**, 027202.
8 T. Lukasczyk, K. Flechtner, L. R. Merte, N. Jux, F. Maier, J. M. Gottfried and H.-P. Steinrück, *J. Phys. Chem. C*, 2007, **111**, 3090–3098.
9 H. Peisert, J. Uihlein, F. Petraki and T. Chassé, *J. Electron Spectrosc. Relat. Phenom.*, 2015, **2014**, 49–60.
10 S. Scheller, M. Goenrich, R. Boecher, R. K. Thauer and B. Jaun, *Nature*, 2010, **465**, 606–608.
11 S. J. Moore, S. T. Sowa, C. Schuchardt, E. Deery, A. D. Lawrence, J. V. Ramos, S. Billig, C. Birkemeyer, P. T. Chivers, M. J. Howard, S. E. J. Rigby, G. Layer and M. J. Warren, *Nature*, 2017, **543**, 78–82.
12 W. Tristan, K. Jörg, E. Ulrich and S. Seigo, *Angew. Chem., Int. Ed.*, 2016, **128**, 10788–10791.
13 K. Zheng, P. D. Ngo, V. L. Owens, X.-P. Yang and S. O. Mansoorabadi, *Science*, 2016, **354**, 339–342.
14 W. Auwärter, D. Écija, F. Klappenberger and J. Barth, *Nat. Chem.*, 2015, **7**, 105–120.
15 J. M. Gottfried, *Surf. Sci. Rep.*, 2015, **70**, 259–379.
16 G. Zamborlini, D. Lüftner, Z. Feng, B. Kollmann, P. Puschnig, C. Dri, M. Panighel, G. Di Santo, A. Goldoni, G. Comelli, M. Jugovac, V. Feyer and C. M. Schneider, *Nat. Commun.*, 2017, **8**, 335.
17 K. Diller, F. Klappenberger, M. Marschall, K. Hermann, A. Nefedov, C. Wöll and J. V. Barth, *J. Chem. Phys.*, 2012, **136**, 014705.
18 S. A. Krasnikov, N. N. Sergeeva, M. M. Brzhezinskaya, A. B. Preobrajenski, Y. N. Sergeeva, N. A. Vinogradov, A. A. Cafolla, M. O. Senge and A. S. Vinogradov, *J. Phys.: Condens. Matter*, 2008, **20**, 235207.
19 T.-C. Tseng, C. Urban, Y. Wang, R. Otero, S. Tait, M. Alcamí, D. Écija, M. Trelka, J. Gallego, N. Lin, M. Konuma, U. Starke, A. Nefedov, A. Langner, C. Wöll, M. Herranz, F. Martin, N. Martin, K. Kern and R. Miranda, *Nat. Chem.*, 2010, **2**, 374–379.
20 A. Calabrese, L. Floreano, A. Verdini, C. Mariani and M. G. Betti, *Phys. Rev. B: Condens. Matter Mater. Phys.*, 2009, **79**, 115446.
21 V. Feyer, O. Plekan, T. Skala, V. Chab, V. Matolin and K. C. Prince, *J. Phys. Chem. B*, 2008, **112**, 13655–13660.
22 S. Fatayer, R. G. A. Veiga, M. J. Prieto, E. Perim, R. Landers, R. H. Miwa and A. de Siervo, *Phys. Chem. Chem. Phys.*, 2015, **17**, 18344–18352.
23 C. Wäckerlin, K. Tarafder, J. Girovsky, J. Nowakowski, T. Hählen, A. Shchyrba, D. Siewert, A. Kleibert, F. Nolting, P. M. Oppeneer, T. A. Jung and N. Ballav, *Angew. Chem., Int. Ed.*, 2013, **52**, 4568–4571.
24 P. Marcus and C. Hinnen, *Surf. Sci.*, 1997, **392**, 134–142.
25 H. Wang, C. Y. Ralston, D. S. Patil, R. M. Jones, W. Gu, M. Verhagen, M. Adams, P. Ge, C. Riordan, C. A. Marganian, P. Mascharak, J. Kovacs, C. G. Miller, T. J. Collins, S. Brooker, P. D. Croucher, K. Wang, E. I. Stiefel and S. P. Cramer, *J. Am. Chem. Soc.*, 2000, **122**, 10544–10552.
26 H. Wang, S. M. Butorin, A. T. Young and J. Guo, *J. Phys. Chem. C*, 2013, **117**, 24767–24772.
27 S. Carlotto, M. Sambi, M. Rancan and M. Casarin, *Inorg. Chem.*, 2018, **57**, 1859–1869.
28 C. Y. Ralston, H. Wang, S. W. Ragsdale, M. Kumar, N. J. Spangler, P. W. Ludden, W. Gu, R. M. Jones, D. S. Patil and S. P. Cramer, *J. Am. Chem. Soc.*, 2000, **122**, 10553–10560.
29 W. Gu, H. Wang and K. Wang, *Dalton Trans.*, 2014, **43**, 6406–6413.
30 S. Rospert, R. Bocher, S. P. J. Albracht and R. K. Thauer, *FEBS Lett.*, 1991, **291**, 371–375.
31 M. Goubeaud, G. Schreiner and R. K. Thauer, *Eur. J. Biochem.*, 1997, **243**, 110–114.
32 Y. Zhou, A. E. Dorchak and S. W. Ragsdale, *Front. Microbiol.*, 2013, **4**, 69.
33 D. Prakash, Y. Wu, S.-J. Suh and E. C. Duin, *J. Bacteriol.*, 2014, **196**, 2491–2498.
34 P. Ge, C. G. Riordan, G. P. A. Yap and A. L. Rheingold, *Inorg. Chem.*, 1996, **35**, 5408–5409.